Air-sea interactions in stable atmospheric conditions: Lessons from the desert semi-enclosed Gulf of Eilat (Aqaba)

Shai Abir[1,2], Hamish A. McGowan[3], Yonatan Shaked[1, 4], Hezi Gildor[1], Morin [1]Efrat, Nadav G. Lensky[1,2]

[1] The Hebrew University of Jerusalem, Jerusalem, Israel.

[2] Geological Survey of Israel, Jerusalem, Israel.

[3] Atmospheric Observations Research Group, The University of Queensland, Brisbane, Australia.

[4] Interuniversity Institute for Marine Sciences, Eilat, Israel.

Correspondence to: Nadav G. Lensky (nadavl@gsi.gov.il)
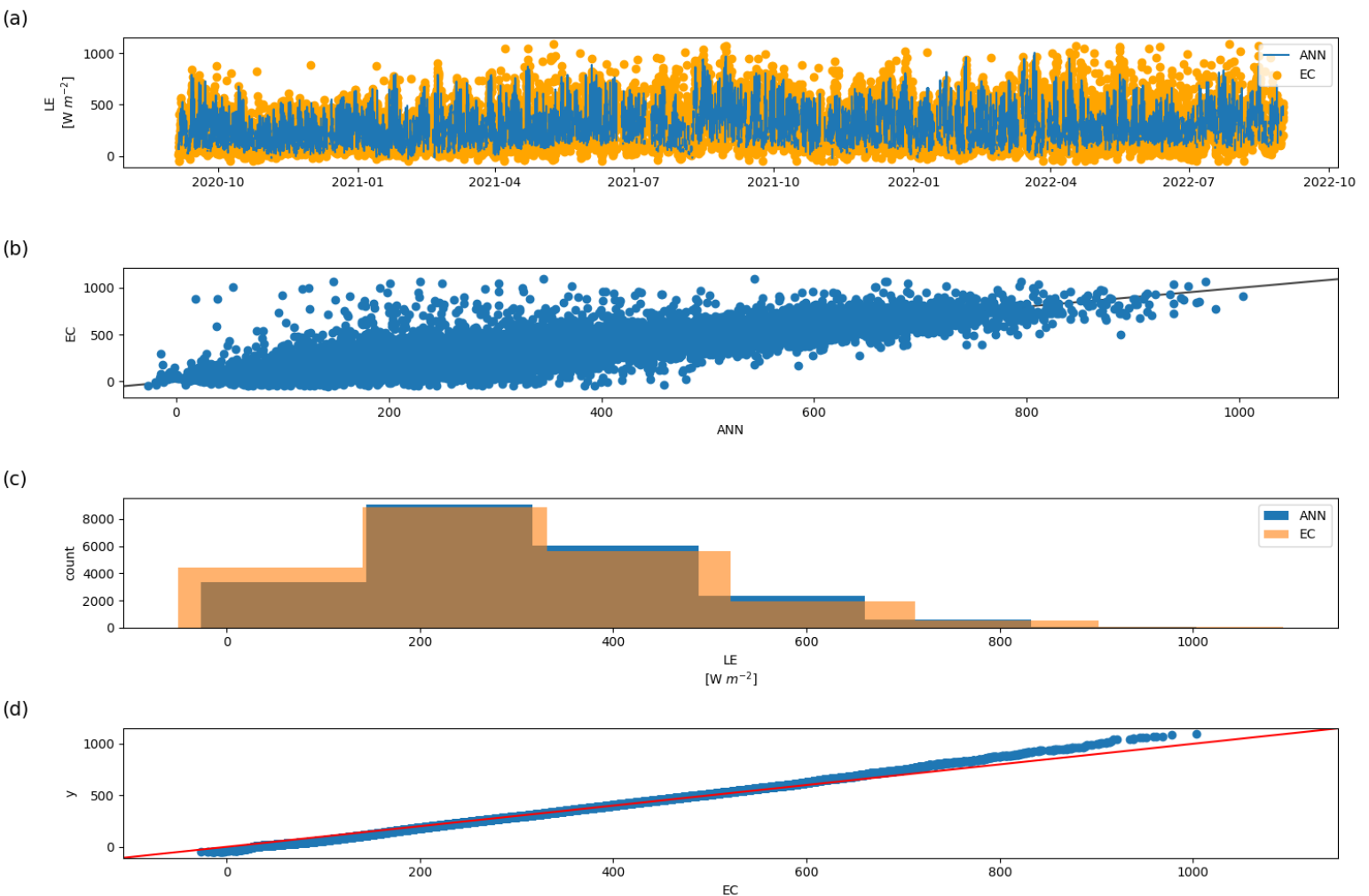
Figure S1: Comparison between the EC-measured latent heat flux and the ANN gap-filling method, units are in W m⁻². (a) Time series comparison, (b) scatter plot comparison (black line is the 1:1 line), (c) histogram of EC measurements and ANN, (d) q-q plot (red line is the 1:1 line). ANN hyperparameters: hidden_layer_sizes= (400,400), max iter=400, learning_rate_init=0.001). R² score and Root Mean Squared Error for the test data set (20% of the data in blocks of 1 week every fifth week) were 0.75 and 95 (W m⁻²) respectively.
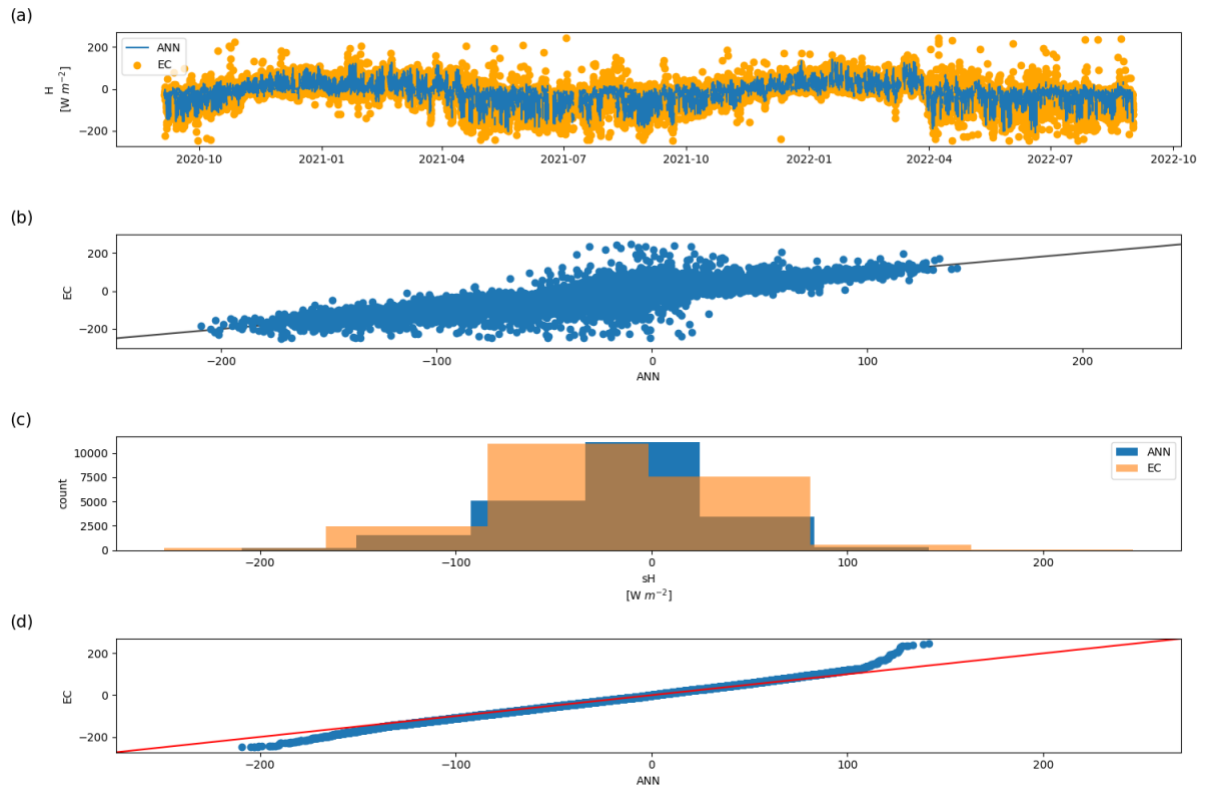
Figure S2: Comparison between the EC-measured sensible heat flux and the ANN gap-filling method, units are in W m⁻². (a) Time series comparison, (b) scatter splot comparison (black line is the 1:1 line), (c) histogram of EC measurements and ANN, (d) q-q plot (red line is the 1:1 line). ANN hyperparameters: hidden_layer_sizes= (400,500), max iter=500, learning_rate_init=0.001). R² score and Root Mean Squared Error for the test data set (20% of the data in blocks of 1 week every fifth week) were 0.79 and 25 (W m⁻²) respectively.
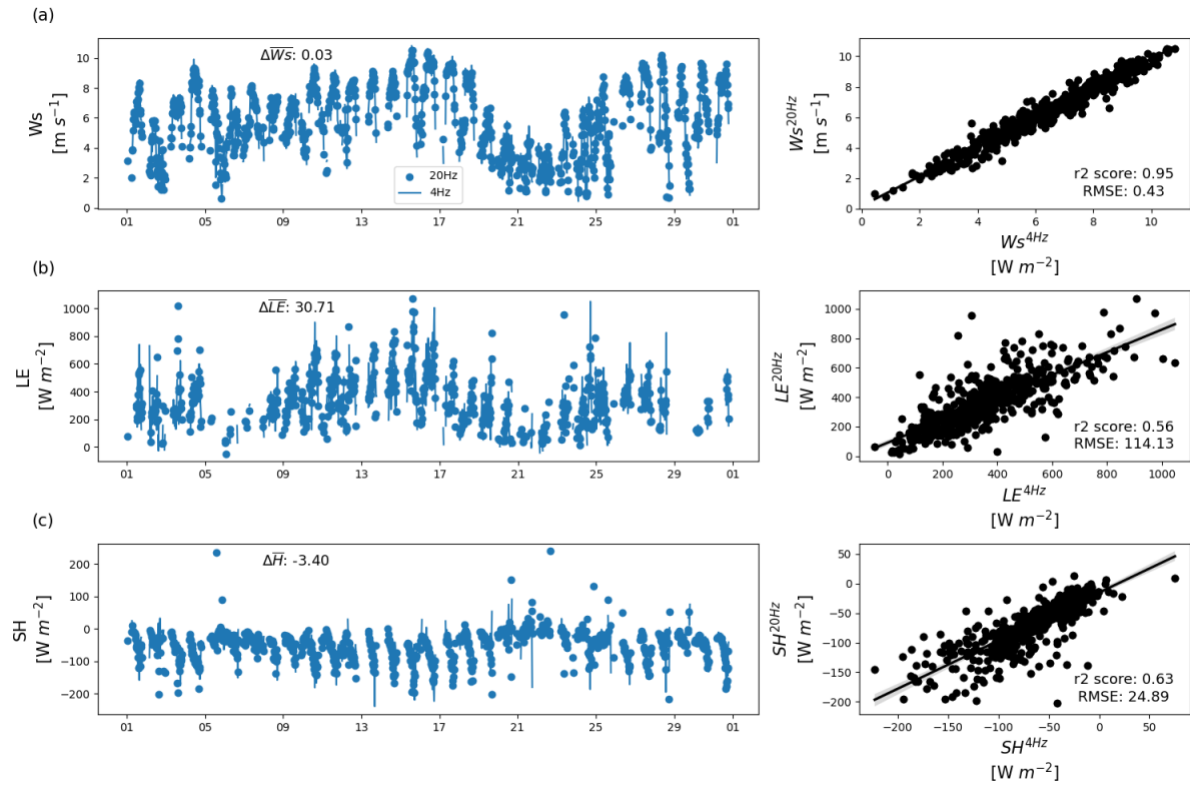
Figure S3: Comparison between the measured fluxes and artificially made downsampled raw EC data to 4 Hz to assess the uncertainty in the flux computation during the period that the station measured in 4 Hz due to an error (April-June 2022), time series (left) and scatter plot (right).
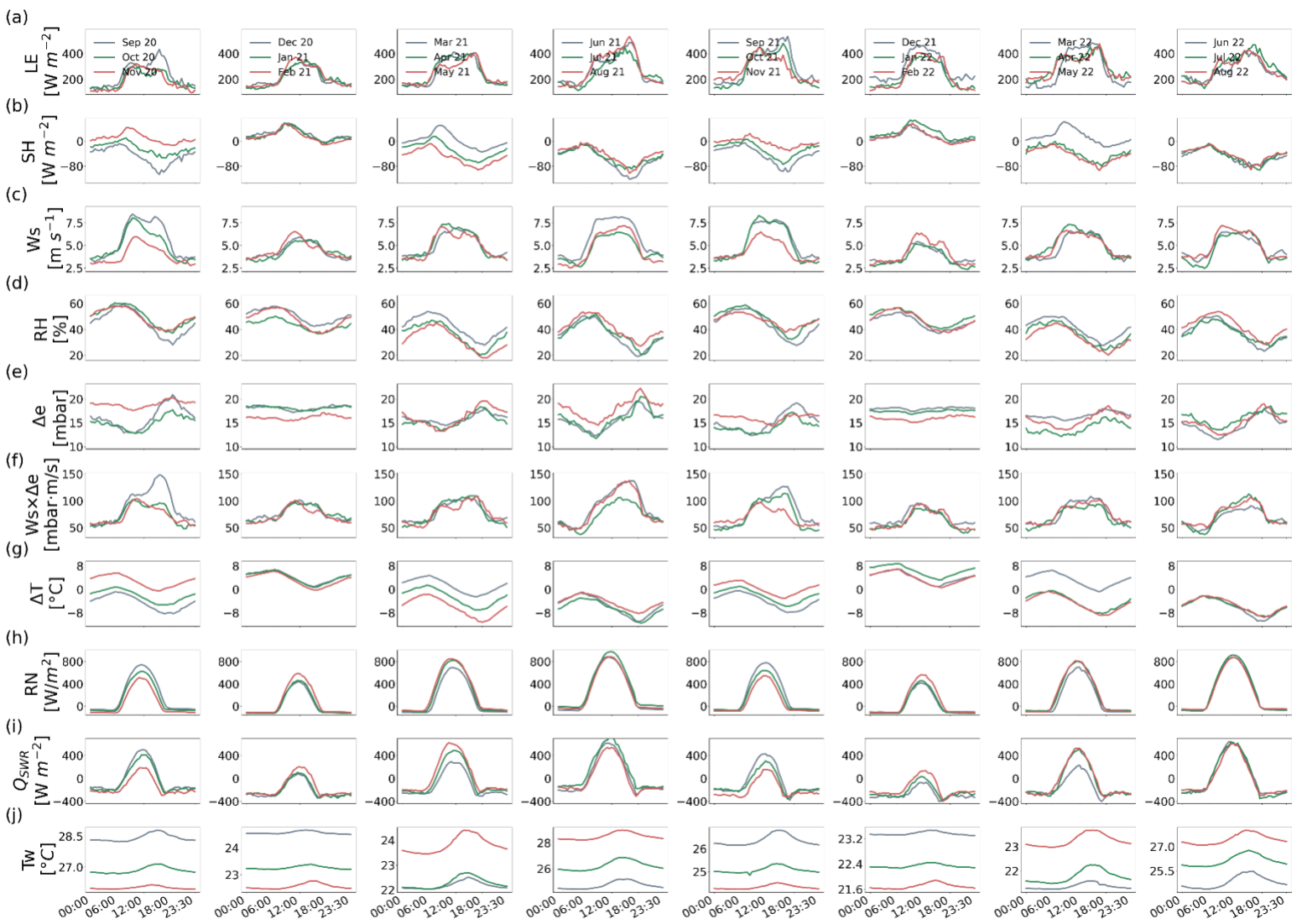
Figure S4: Monthly mean diurnal cycle of micrometeorological and flux variables divided into seasons (Winter=DJF, Spring=MAM, Summer=JJA, Autumn=SON). (a) Latent heat flux (LE), (b) Sensible Heat flux (SH), (c) Wind speed (Ws), (d) Relative humidity (RH), (e) Vapor pressure difference (Δe), (f) Wind speed and vapor pressure difference product ($Ws \times \Delta e$), (g) water-air temperature difference (ΔT), (h) Net radiation (RN), (i) Sea water residual (Q_{SWR}) (j) Water temperature (Tw).
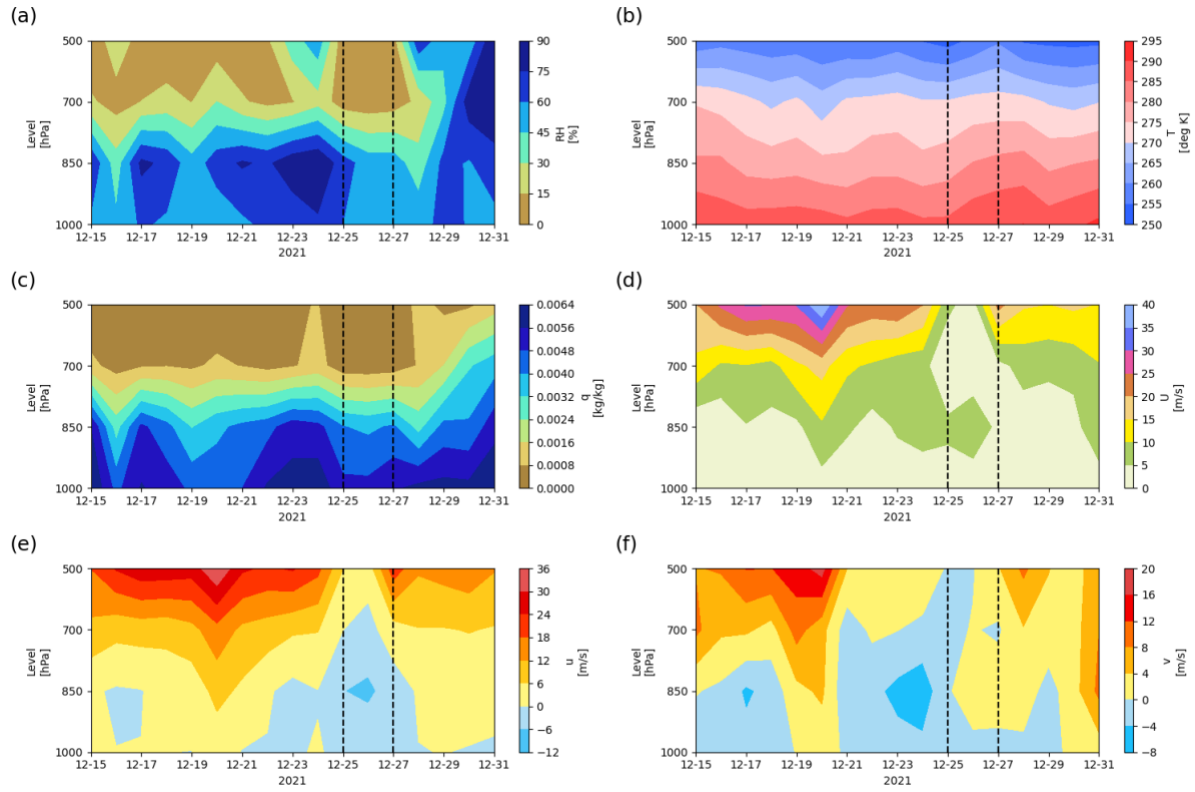
Figure S5: Vertical profile of the daily averaged ERA-5 pressure level hourly data (Hersbach et al., 2023b, 2023a) at the closest gridpoint to the IUI station (29N, 35E). (a) relative humidity, (b) air temperature, (c) specific humidity, (d) wind speed, (e) u-component of the wind, (f) v- component of the wind. The profiles show intensification of the western component of the winds specifically at 850 hPa, lower relative humidity values.

Evaluating how the travel distance of the wind over the sea affect heat exchange

To evaluate how the heat exchange will change along the GoE where in the southern areas the wind travels a longer distance over the sea; we examine how the heat exchange varies in the rarer times where a synoptic state leads to southerly winds which travel a longer distance than the dominant northerly winds. This analysis is conducted in winter months (DJF) as southerly winds are more common in the winter season due to regional synoptic.

When the wind is originated from the sea (135-260º), the wind speed is weaker by ~0.7 m s^{-1} however, with two times larger range of 1 SD (Fig S6). Relative humidity exhibits similar behavior but of an opposing trend- when the wind is sea-originated the relative humidity is higher (51% during the sea-originated direction in comparison to 47% during the northerly winds) due to the longer travel time over water. The lower wind speed and higher humidity result in an average reduction of 3 mbar and 33 W m^{-2} in the mean diurnal cycle of the vapor pressure difference and latent heat flux, respectively in the sea-originated wind occasions. The water and air temperature difference demonstrates a 3.35 ºC variation through the mean diurnal cycle with a mean temperature difference of 2.03 ºC. In comparison during normal flow days, the water and air temperature difference mean diurnal variations are in a magnitude of 6.06 ºC with a mean value of 4.36 ºC; which is a result of the higher air temperature in the sea-originated flow. Ultimately the dumping of the gradient and the weaker winds during sea-originated winds results in an average 21 W m^{-2} reduction in the mean diurnal cycle of the sensible heat.

When wind originates from the north the air temperature and relative humidity portrayed high diurnal variation which is more typical of terrestrial boundary layer characteristics (Pal Arya, 1988). When the wind was blowing from the south, air temperature and relative humidity had smaller diurnal variations, and the water-air temperature difference decreased. This reduces the sensible and latent heat fluxes at our measurements site. However, it is difficult to determine if there would be an actual significant reduction due to spatial wind speed variations throughout the GoE and the large overlap between the 1 SD range from the mean between the two flow types. Above the open sea and in the southern wider parts of the GoE wind speed increases (Berman et al., 2000) due to the lower roughness of the sea surface than the lands (Pal Arya, 1988). To resolve the spatial distribution of heat fluxes multiple EC station comparison is needed or a Lagrangian approach of a vessel-mounted EC station.
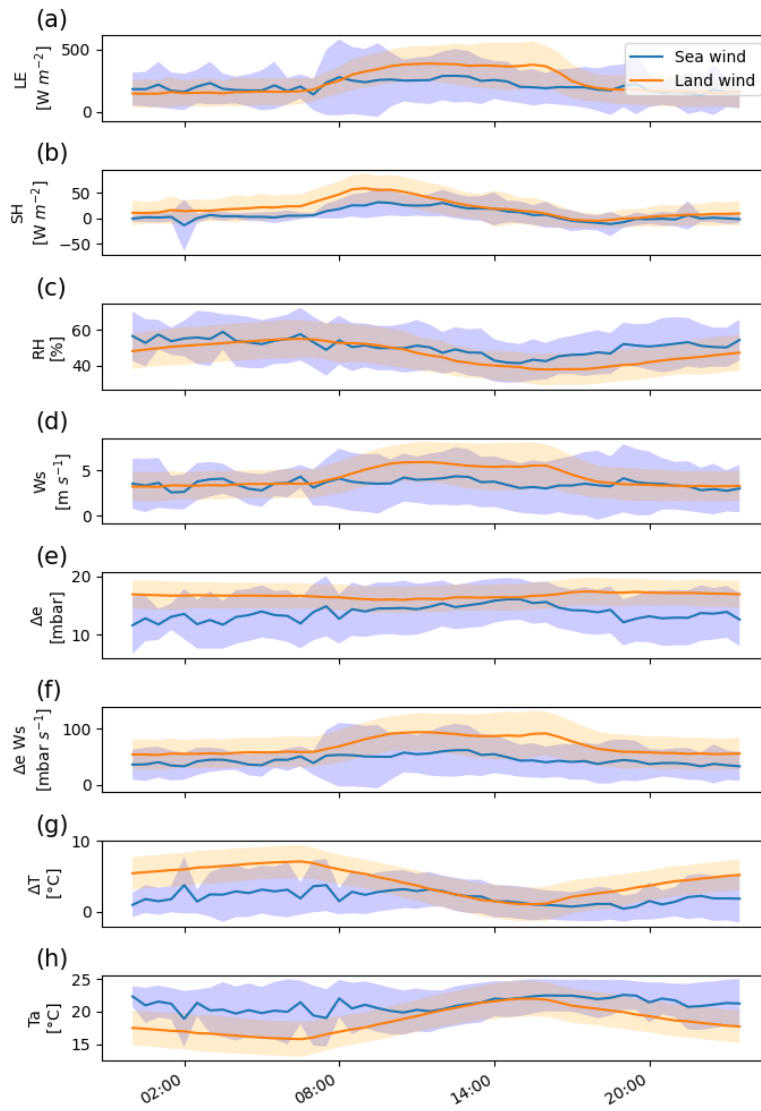
Fig S6. Comparison of the mean diurnal cycle of the heat fluxes and micrometeorology divided by sea-originating wind and land-origination wind (the shaded area corresponded to the +/- 1 sd.). Sea winds 135<= wind direction <=260 deg from the north (to compare southerly winds with long travel time over the sea) and the rest is land-originated wind (DJF only). (a) Latent heat, (b) sensible heat, (c) relative humidity, (d) wind speed, (e) vapor pressure difference, (f) vapor pressure difference and wind speed product, (g) water and air temperature difference, (h) air temperature.

Heat storage calculation

The data was collected by an RBRconcerto³ CTD, mounted on a wave-driven vertical profiler. Profiles (ascending profiles only where used) of derived salinity and measured temperature at a frequency of 8 Hz were recorded. Each profile was de-spiked (threshold=4.0, windowLength=11), bin averaged (bunBy=depth, boundary=[0.5,145]) using the pyrsktools python library, such as the resulting profiles are from 0.5-145 meters at 1-meter intervals. For the calculation of the heat storage, the temperature profile was smoothed using python scipy.signal library savgol_filter function (window_length=5, polyorder=3) and then interpolated to fill missing NAN. The total heat of the water column of each preprocessed CTD profile was then computed according to the:

$$Hg = \rho \cdot C_p \cdot \overline{T} \cdot \Delta Z \tag{1}$$

Where Hg is the total heat of the profile water column in Jm^{-2}, ρ is the seawater density, and C_p is the heat capacity at a constant pressure of seawater ($\rho \cdot C_p = 4.1 \cdot 10^6 [Jm^{-3\circ}C^{-1}]$) (Each profile was assigned the mean timestamp of the profile), $\overline{T}$ is the mean temperature of each 1-meter water layer in the profile and ΔZ is the 1-meter water layer thickness. The total heat was downsampled to a 1-hour frequency (for sensitivity check we changed the temporal resolution to 1 day which resulted in 3% change in the mean heat storage change) with a weighted average algorithm (mean time between profiles is ~22 minutes) and then underwent a rolling averaged procedure with a 2-day centered window to eliminate internal wave oscillation in the data. The total heat was then smoothed with a savgol filter (window_length=15, polyorder=3). Lastly, the change in heat storage was calculated:

$$G = \frac{\Delta Hg}{\Delta t} \tag{2}$$

Where G is the change in heat storage in W m^{-2}, ΔHg is the change in total heat between adjacent profiles, and the Δt in second is the time between them (1 hour).

Calculating atmospheric stability

In this section, the calculation method for the atmospheric stability parameter is explained. The COARE3.6 algorithm (Fairall et al., 1996) utilizes the following formula for the atmospheric stability (ζ) (after using an initial guess by the bulk Richardson number):

$$\zeta = z_r/L \tag{3}$$

Where z_r is the atmospheric reference height and L is the Monin Obukhov length, which is calculated as:

$$L = \frac{kg}{T}(T_* + 0.61Tq_*)/u_*^2 \tag{4}$$

Here k is the von Kerman constant, g is the gravity acceleration, T is the air temperature and T_*, q_*, u_* are the scaling parameter for temperature humidity and wind speed (friction velocity). (Eq. 9 in Fairall et al. (1996)).

On the contrary the calculation L and so ζ by the Eddypro© program is relying on the directly computed friction velocity and sensible heat both available from the 3D wind anemometer measurement:

$$L = -\frac{\Theta_p u_*^3}{kg\frac{H_0}{\rho_a C_p}}$$

(5)

Where Θ_p is the potential temperature, H_0 is the uncorrected sensible heat flux, ρ_a, C_p are the air density and Air heat capacity at constant pressure, and here u_* is the friction velocity.

Reference

Berman, T., Paldor, N., & Brenner, S. (2000). Simulation of wind-driven circulation in the Gulf of Elat Aqaba. In Journal of Marine Systems (Vol. 26). www.elsevier.nlrlocaterjmarsys

EddyPro® 7 Software: Express default settings: https://www.licor.com/env/support/EddyPro/topics/express-defaults.html, last access: 13 June 2023.

Fairall, C. W., Bradley, E. F., Rogers, D. P., Edson, J. B., and Young, G. S.: Bulk parameterization of air-sea fluxes for tropical ocean-global atmosphere coupled-ocean atmosphere response experiment, J Geophys Res Oceans, 101, 3747–3764, https://doi.org/10.1029/95JC03205, 1996.

Hersbach, H., Bell, B., Berrisford, P., Biavati, G., Horányi, A., Muñoz Sabater, J., Nicolas, J., Peubey, C., Radu, R., Rozum, I., Schepers, D., Simmons, A., Soci, C., Dee, D., & Thépaut, J.-N. (2023a). ERA5 hourly data on pressure levels from 1940 to present. In Copernicus Climate Change Service (C3S) Climate Data Store (CDS). https://doi.org/10.24381/cds.68d2bb30

Hersbach, H., Bell, B., Berrisford, P., Biavati, G., Horányi, A., Muñoz Sabater, J., Nicolas, J., Peubey, C., Radu, R., Rozum, I., Schepers, D., Simmons, A., Soci, C., Dee, D., & Thépaut, J.-N. (2023b). ERA5 hourly data on single levels from 1940 to present. In Copernicus Climate Change Service (C3S) Climate Data Store (CDS).

Pal Arya, S. (1988). Introduction to micrometeorology. Academic Press, Inc.